

4-21-2005

Atomistic Approach for Nanoscale Devices at the Scaling Limit and Beyond - Valley Splitting in Si

Anisur Rahman

Purdue University - Main Campus

Gerhard Klimeck

Purdue University - Main Campus, gekco@purdue.edu

Mark Lundstrom

Purdue University - Main Campus

Timothy Boykin

The University of Alabama, Huntsville

Nizami Vagidov

State University of New York

Follow this and additional works at: <http://docs.lib.purdue.edu/nanodocs>

Rahman, Anisur; Klimeck, Gerhard; Lundstrom, Mark; Boykin, Timothy; and Vagidov, Nizami, "Atomistic Approach for Nanoscale Devices at the Scaling Limit and Beyond - Valley Splitting in Si" (2005). *Other Nanotechnology Publications*. Paper 126.

<http://docs.lib.purdue.edu/nanodocs/126>

This document has been made available through Purdue e-Pubs, a service of the Purdue University Libraries. Please contact epubs@purdue.edu for additional information.

Atomistic Approach for Nanoscale Devices at the Scaling Limit and Beyond— Valley Splitting in Si

Anisur RAHMAN, Gerhard KLIMECK*, Mark LUNDSTROM, Timothy B. BOYKIN¹ and Nizami VAGIDOV²

School of Electrical and Computer Engineering, Network for Computational Nanotechnology Purdue University, West Lafayette, IN 47907, USA

¹Department of Electrical and Computer Engineering, University of Alabama, Huntsville, AL 35899, USA

²Department of Electrical Engineering, State University of New York, Buffalo, NY 14260, USA

(Received September 21, 2004; accepted January 6, 2005; published April 21, 2005)

Band-structure effects on channel carrier density in the ultrathin-body end of the ITRS roadmap silicon (100) n-type metal oxide semiconductor field effect transistors (MOSFETs) are assessed here using a semi-empirical nearest-neighbor $sp^3d^5s^*$ tight-binding model with spin-orbit interaction. The calculations focus on the body thickness range between 10 and 18 atomic layers (~ 1.5 – 2.5 nm). At this range, the standard effective mass approach is limited by its inability to capture the conduction band nonparabolicity effects and the subband splitting. The tight-binding simulations show interesting effects of ground-state subband splitting in this thickness range, and as a result of this, the channel charge density was found to fluctuate by as much as 30%. Additionally, it was observed that strict process tolerance is necessary in this thickness range in order to maintain an acceptable threshold voltage variation. [DOI: 10.1143/JJAP.44.2187]

KEYWORDS: ultra-thin-body Si, valley splitting, bandstructure, tight-binding, charge fluctuation

1. Introduction

Over the past three decades, metal oxide semiconductor field effect transistors (MOSFETs) have been scaled down aggressively. According to the ITRS 2001 roadmap projection, devices in the 2016 will have channel lengths of 10 nm. New device geometries must be explored to ensure electrostatic control. Thin semiconductor-on-insulator (SOI) and Ge channel devices are considered in this regard. Design studies of such devices have revealed that in order to curb short channel effects, their body thickness should not exceed 2–3 nm.^{1,2)} For such an extremely thin body, the underlying atomistic texture makes the use of the ubiquitous effective mass (EM) approach questionable and an atomistic treatment of the device becomes essential. Here the semi-empirical tight-binding (TB) theory is applied to semiconductor thin films on (100) wafers and the subband structure as well as the effect of valley interaction are investigated.

2. Approach

In this work, we explore the band-structure effects in the ultrathin-body (UTB) silicon n-MOSFETs on (100) wafers. The underlying atomic structure is schematically presented in Fig. 1. The crystal structure for cubic semiconductors is the FCC lattice with two atoms associated with each lattice point—the lattice atom at the lattice site and the basis atom a quarter of the body diagonal away. For elemental semiconductors (*e.g.*, Si, Ge) these two are of the same atomic type, however, for compound semiconductors (*e.g.*, GaAs, InP), they are of different types of atoms. For a (100) wafer, the channel is formed by alternatively stacking such atomic layers. In this figure, they are shown by layers of black and white circles, respectively.

The band-structure of the thin silicon channel is explored using a $sp^3d^5s^*$ tight-binding (TB) model.³⁾ This is an atomistic approach, which offers a balance between treating the finite atomic resolution at this scale and the convenience of device simulation. Here, each atomic layer is modeled by

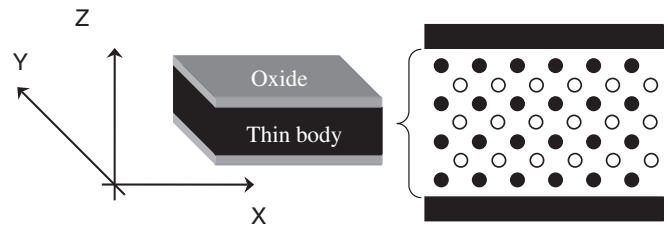


Fig. 1. The thin film on (100) wafers modeled in this work. The film is composed of two types of alternately repeating atomic layers: lattice atoms (black) and basis atoms (white).

ten atomlike orbitals for each spin. Spin-orbit coupling is used in all simulations and therefore, each atomic layer contributes a 20×20 block to the thin-film Hamiltonian. Only the nearest-neighbor interaction is treated, therefore, the thin-film Hamiltonian becomes block tridiagonal. The atomistic representation of the channel along Z causes the Hamiltonian to be a function of only the wave vector, k_{\parallel} , which runs parallel to the channel-oxide interface. The model allows us to explore the thin-film band-structures with even as well as odd numbers of atomic layers. The orbital interaction energies are optimized to give accurate band gaps and effective masses for the lowest lying conduction band valleys and valence bands in bulk silicon.³⁾

In an UTB dual-gate (DG) silicon MOSFET, the channel is sandwiched between two thin gate oxide layers and therefore, the carrier motion is restricted along the thickness direction. In this work, the zero boundary condition of the associated wave function is assumed at the top and the bottom silicon-oxide interface. The mismatch between bonds in silicon and oxide layers results in dangling bonds and forms surface states in semiconductor devices. Experimentally, these surface states are pacified by hydrogen absorption. In these simulations, we use the boundary condition described in⁴⁾ to model pacification of the dangling bonds. The subbands are the stationary states formed in this quantum well due to energy quantization along the thickness direction. A typical TB ground-state wave function for the silicon subband is presented in Fig. 2 where the atomistic

*Corresponding author. E-mail address: gekco@purdue.edu

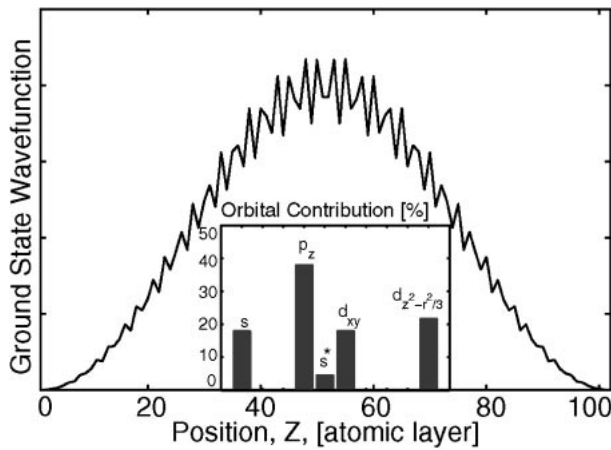


Fig. 2. Typical TB wave function in Si (100) films. The sum of squared orbital contribution is plotted. Inset: The individual orbital contribution. Only the orbitals shown contribute to the wave function.

nature is clearly visible. The carriers are free to move in the X-Y plane, and the associated motion results in current in a device.

3. Results and Discussion

In Fig. 3, the ground-state energy is plotted as a function of body thickness. The results obtained using the $sp^3d^5s^*$ -SO tight-binding model (symbols) and the EM approach (dashed) are presented in this figure. In the thick body limit, as expected, the ground-state energy approaches the bulk conduction band edge. It can be seen that for a body thickness of 25 atomic layers (~ 3.5 nm) or more, the results of the EM approach agrees well with tight-binding results. However, for thinner bodies, TB results show two interesting features that are otherwise not revealed by the EM approach. First, the nonparabolicity of the E-k relationship along [001]

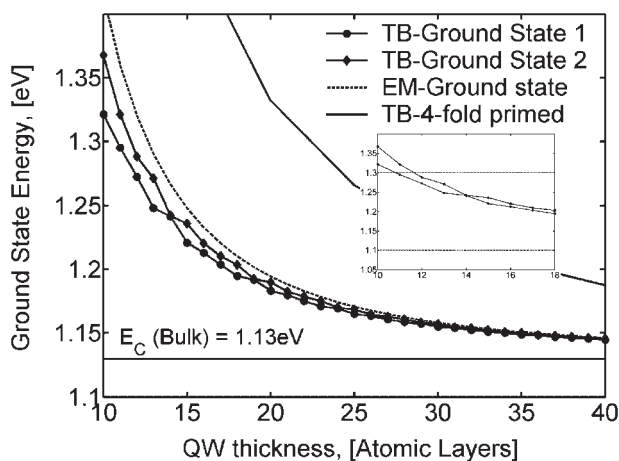


Fig. 3. The ground-state energy vs body thickness calculated using the $sp^3d^5s^*$ -SO tight-binding model and the EM approach. Below a thickness of 25 atomic layers, two effects are seen in TB results which are not apparent in the EM result. First, the nonparabolicity of the E-k relationship along lowers the TB subband energies. Second, the interaction between the two conduction band ellipsoids splits the ground-state energy. In the EM approach, such an interaction is absent and the ground state is twofold degenerate. The ground-state of the fourfold degenerate primed ladder is also plotted (solid). Inset: TB ground-state energies for thickness of 10–18 atomic layers.

lowers the TB subband energies. Secondly, in TB results, the interaction between the two conduction band ellipsoids splits the ground-state subband edge. In the EM approach, this interaction is absent and the ground state is twofold degenerate. This work focuses is on the end devices of the ITRS roadmap, which have to body thicknesses of 1.5–2.5 nm (~ 10 –18 atomic layers). The ground state of the fourfold degenerate primed subband ladder is also plotted in this figure. These subbands are formed by the four inplane valleys which have smaller transverse effective mass along the quantum well thickness direction, and hence, such subbands are higher in energy. The inset shows the ground-state energies in this thickness range, obtained by tight-binding calculation. Two horizontal lines at $E = 1.1$ and 1.3 eV represent the non-degenerate and degenerate injector Fermi levels which are used in Figs. 8–9.

It is observed in Fig. 3 that for very thin channels, the ground-state subbands in silicon are no longer twofold degenerate, but the interaction between the valleys causes them to split in energy. For thicker bodies, this splitting is negligible, however, it becomes considerable for body thickness below 20 atomic layers. In Fig. 4, this ground-state splitting is plotted as a function of quantum well thickness, calculated using the tight-binding model. The odd and even numbers of atomic layers show similar splitting profiles. This is not obvious in the inset where the odd and even numbers of layers are not distinguishable from each other. The origin of subband splitting is schematically presented in Fig. 5. The bulk Brillouin zone is shown on the left and E - k along at $k_x = k_y = 0$ is shown on the right. The black and white circles represent four traveling states around the two band minima which combine to form two subbands. At small body thickness, these states move to higher energy and the interaction between them becomes stronger. This interaction is the cause of subband splitting.^{5,6)}

Using the tight-binding model, the E - k relationship is calculated over the entire two-dimensional Brillouin zone and the data are converted to the densities of states. In Fig. 6, the 2D density of states vs energy plots are presented for body thicknesses between 10 and 18 atomic layers. At room temperature, valley splitting as large as $2k_B T$ is

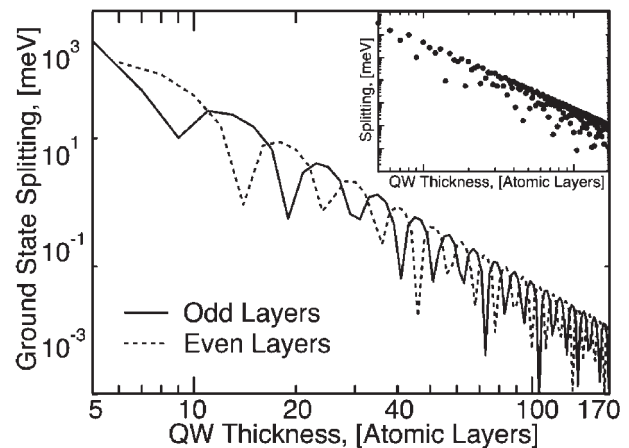


Fig. 4. The splitting vs quantum well thickness in silicon using TB. The odd and even numbers of atomic layers show similar splitting profiles. This is not obvious in the inset where the odd and even numbered layers are not distinguishable from each other.

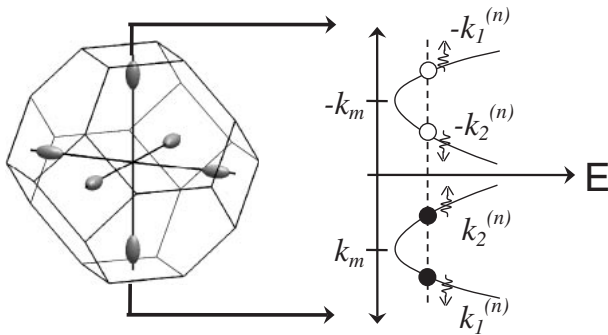


Fig. 5. The origin of subband splitting. The bulk Brillouin zone is shown on the left and the $E-k$ along at $k_x = k_y = 0$ is shown on the right. The black and white circles represent four traveling states around the two band minima which combine to form two subbands. At small body thickness, these states move to higher energy and the interaction between them becomes stronger. This interaction is the cause of subband splitting.⁵⁾

observed, which significantly alters the band-structure at the subband edge. For the 14 atomic layers (~ 2 nm) channel, valley splitting is practically zero, however, it abruptly increases for both higher and lower thicknesses.

Figure 7 shows the effects of ground-state splitting on carrier densities at three different temperatures: 300, 77 and 4 K. Here, for each body thickness, the Fermi level is placed exactly at the lower ground-state subband edge. As a result, the variation of carrier densities in these tuned devices is a direct consequence of subband splitting. It is observed that the effect of subband splitting on carrier density can be as high as 30%.

The effect of the injector (source or drain in MOSFETs) Fermi level on the channel carrier density is shown in Figs. 8–9. Here, the equilibrium channel charge is calculated

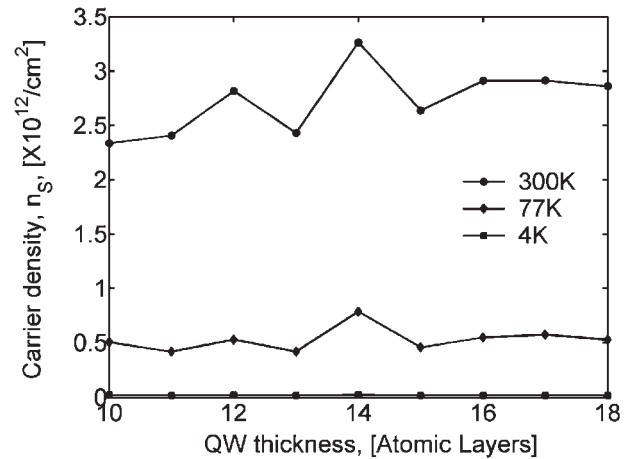


Fig. 7. Effect of ground-state splitting on carrier density at 300, 77 and 4 K. For each body thickness, the Fermi level is placed at the lower of the two ground-state energies. The difference in carrier density is a direct consequence of subband splitting.

using two different injector Fermi levels. For a degenerately doped ($\sim 10^{18}/\text{cm}^3$) injector, the Fermi level is above the bulk band edge (1.13 eV). In Fig. 8, carrier density vs body thickness is plotted at this limit. Here, the Fermi level is fixed at $E_F = 1.3$ eV, which is close to or above the lowest channel subband, and the inversion layer charge is calculated in the silicon channel using the 2D tight-binding band-structure. The strong effect of body thickness on charge density is apparent in this plot.

Finally, the calculations used in the case of Fig. 8 are repeated for Fig. 9 in the limit where the injector is nondegenerately doped. In this figure, the Fermi level is placed well below the subband edge, at $E_F = 1.1$ eV. In this

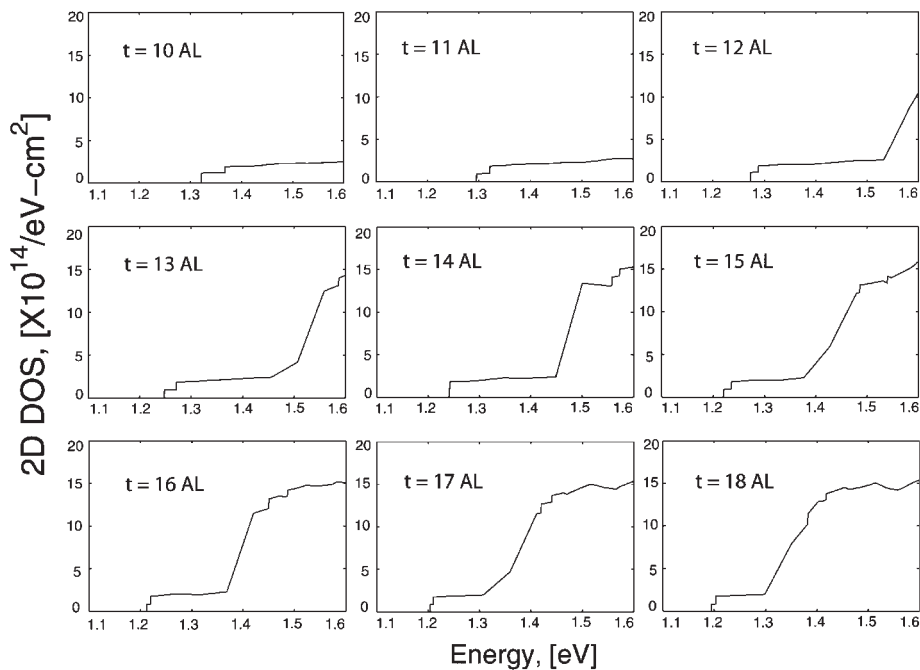


Fig. 6. The 2D density of states vs energy plots for body thicknesses between 10 and 18 atomic layers. The strong first subband splitting is visible in the plots. At 14 atomic layers (~ 2 nm), splitting is practically zero, however, it abruptly increases in both directions.

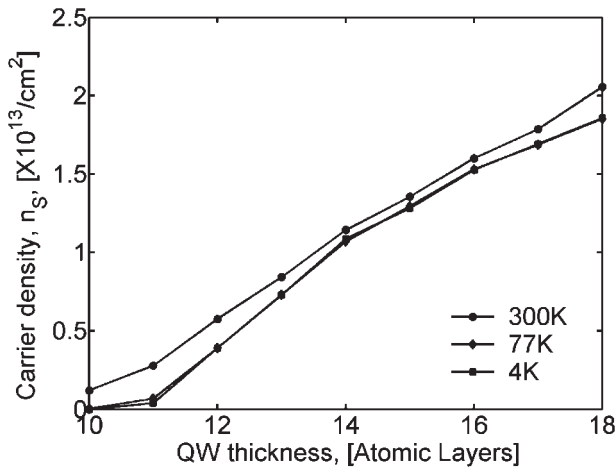


Fig. 8. Carrier density vs body thickness in the degenerate injector (source/drain) limit. Here the Fermi level is fixed at $E_F = 1.3$ eV and the inversion layer charge is calculated in the silicon channel using the 2D tight-binding band-structure. The strong effect of body thickness on charge density is apparent.

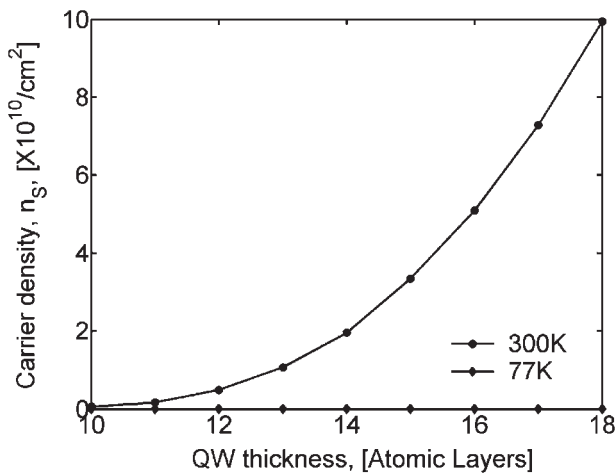


Fig. 9. Carrier density vs body thickness in the nondegenerate injector limit. The Fermi level is placed well below the subbands, $E_F = 1.1$ eV. The channel is depleted of carriers and this resembles the off-state for a MOSFET. At 300 K, the channel charge depends strongly on the body thickness and therefore, a strict process tolerance is necessary to ensure an acceptable threshold voltage.

limit, the channel is populated by carriers with energies in the tail of the Fermi function. This resembles the depleted channel at the off-state of a MOSFET. The strong variation of charge density with body thickness reveals that a strict

process tolerance is necessary at this thickness limit to ensure an acceptable threshold voltage. In Figs. 7–9, carrier density is calculated by integrating densities over the entire 2D Brillouin zone, and therefore, they also include the carriers residing in the upper subbands and in the fourfold degenerate primed subband ladder. In Figs. 7 and 9, such subbands are much higher compared to the Fermi Energy, and therefore, are practically empty. In the degenerate injector limit (Fig. 8), they contribute to charge density only for body thickness of 17 and 18 atomic layers, however, such contribution is a small fraction of the total charge density.

4. Conclusion

In this work, we explored the band-structure effects in ultrathin-body Si n-MOS devices using an atomistic tight-binding model. In order to include the correct effective masses and band gaps of the indirect band gap material, Si, in the model, the $sp^3d^5s^*$ basis set with spin-orbit interaction was used. The simulation revealed interesting features in the MOSFETs at the scaling limit, which otherwise are not captured by the traditional EM approach. Valley interaction causes the removal of subband degeneracy, which may have crucial effect on the transport properties of CMOS devices at the end of the roadmap and beyond. Additionally, a stringent process tolerance was found to be a key issue at this body-thickness limit, since even a variation of one monolayer changes the threshold voltage considerably, resulting in a large variance in V_T .

Acknowledgement

This research has been carried out under SRC contract no. 1042 and NSF contract no. EEC-0228390.

- 1) S. Hasan, J. Wang and M. Lundstrom: *Solid-State Electron.* **48** (2004) 867.
- 2) A. Rahman, A. Ghosh and M. Lundstrom: *Tech. Dig. Int. Electron Devices Meet.* (2003) 19.4.1.
- 3) T. B. Boykin, G. Klimeck and F. Oyafuso: *Phys. Rev. B* **69** (2004) 115201.
- 4) S. Lee, F. Oyafuso, P. von Allmen and G. Klimeck: *Phys. Rev. B* **69** (2004) 045316.
- 5) T. B. Boykin, G. Klimeck, M. A. Eriksson, M. Friesen, S. N. Coppersmith, P. von Allmen, F. Oyafuso and S. Lee: *Appl. Phys. Lett.* **84** (2004) 115.
- 6) T. B. Boykin, G. Klimeck, M. Friesen, S. N. Coppersmith, P. von Allmen, F. Oyafuso and S. Lee: *Phys. Rev. B* **70** (2004) 165325.